Sectional distribution patterns of Cd, Ni, Zn, and Cu in the North Pacific Ocean: Systematic importance of scavenging

L. Zheng[1*], T. Minami[2], S. Takano[1], T.Y. Ho[3, 4] and Y. Sohrin[1]

[1]Institute for Chemical Research, Kyoto University, Uji, Kyoto 611-0011, Japan

[2]Engineering and Technology Department, Kanazawa University, Kanazawa, Ishikawa 920-1192, Japan

[3]Research Center for Environmental Changes, Academia Sinica, Taipei, Taiwan

[4]Institute of Oceanography, National Taiwan University, Taipei, Taiwan

Corresponding author: Linjie Zheng (zheng.linjie.7w@kyoto-u.ac.jp)

Key Points:

- Basin-scale full-depth sectional distributions of total dissolvable, dissolved, and labile particulate Cd, Ni, Zn, and Cu are observed in the North Pacific Ocean.
- Cd is predominantly controlled by biogeochemical cycling, and the stoichiometry with major nutrients is modified *via* ocean circulation.
- Ni, Zn, and Cu are accumulated in the Pacific Deep Water due to scavenging and redissolution from sinking particles and sediments.

Abstract

The North Pacific Ocean is the largest basin and is located at the end point of the thermohaline circulation of deep water. Few concurrent data of cadmium (Cd), nickel (Ni), zinc (Zn), and copper (Cu) in seawater have been reported in this area so far. Herein, we report the basin-scale full-depth sectional distributions of the total dissolvable, dissolved, and labile particulate Cd, Ni, Zn, and Cu along the 160°W, 165°E (GP18), and 47°N (GP02) GEOTRACES transects. Our data reveal that the relations of the four dissolved metals (dMs) with $Si(OH)_4$ and PO_4 considerably differ from those in other oceans. The plot of the preformed Cd vs. the preformed PO_4 exhibits strong linearity and passes an origin. Moreover, the dCd/PO_4 ratio is 0.34 ± 0.02 mmol/mol ($n = 296$) at a depth lower than 800 m, which is in the range of the phytoplankton Cd/PO_4 ratio, thus indicating the dominant effect of the biogeochemical cycling on the dCd distribution. The dMs/PO_4 ratios of the other examined metals are partially or completely out of the phytoplankton ratios and generally increase with depth in waters deeper than 800 m. Specifically, the increase is the strongest for Cu and moderate for Ni and Zn. The dMs/PO_4 ratios below 800 m decrease with the apparent oxygen utilization increasing from 150 to 300 μmol/kg by 4% for Cd, 21% for Zn and Ni, and 69% for Cu. We thus demonstrate that scavenging is an important factor that significantly affects the distributions of Zn, Ni, and Cu, whereas the effect increases in the order Cd < Ni, Zn < Cu.

1 Introduction

Trace metals that have nutrient-type distributions are actively taken up by phytoplankton in surface waters, sink to the depth with settling particles, and are released from the particles *via* the oxidative decomposition of organic matter and the dissolution of minerals, such as silica and carbonates (Broecker & Peng, 1982; Elderfield, 2003). This mechanism is called as marine biogeochemical cycling. Cadmium (Cd), nickel (Ni), zinc (Zn), and copper (Cu) are classified as nutrient-type or recycle-type trace metals (Bruland, Orians, & Cowen, 1994; Whitfield & Turner, 1987), which act as essential cofactors in metalloenzymes and thus control the metabolism of organisms (Sunda, 1989; Twining & Baines, 2013). In turn, the oceanic phytoplankton community significantly affects the concentrations and cycling of the trace metals in the ocean (Sunda, 2012).

The concentration of the nutrient-type metals generally increases with the age of deep water from the Atlantic Ocean through the Southern Ocean and ultimately to the Indian Ocean and Pacific Ocean. For example, the bottom water concentration of dissolved Cu (dCu) increases with the flow path of deep water and reaches ca. 1.3 nmol/kg in the Northeast Atlantic Ocean (Danielsson, Magnusson, & Westerlund, 1985), ca. 3 nmol/kg in the Southern Ocean (Heller & Croot, 2015; Monteiro & Orren, 1985), and ca. 5 nmol/kg in the Indian Ocean (Vu & Sohrin, 2013) and the Pacific Ocean (Bruland, 1980). The concentration of dCu increases from surface to bottom by around five times in the Pacific Ocean (Bruland, 1980) and only by 10% in the Atlantic Ocean (Danielsson et al., 1985). The oceanic circulation affects not only the concentrations of the nutrient-type metals but also their ratios against major nutrients. The mole ratio of dCd/PO_4 exhibits significant spatial variations (Löscher, de Jong, & de Baar, 1998; van der Loeff, Helmers, & Kattner, 1997). In this paper, Cd/PO_4 is employed to indicate a spot ratio, and $Cd:PO_4$ to denote either a slope of the regression line in the Cd vs. PO_4 plot, which indicates

an uptake, or a remineralization ratio in accordance with the definition reported in the literature (Middag, van Heuven, Bruland, & de Baar, 2018; Quay, Cullen, Landing, & Morton, 2015). Elderfield and Rickaby (Elderfield & Rickaby, 2000) compiled global data and found that the dCd/PO_4 (mmol/mol) ratio in surface water increases with latitude. Whereas this ratio in deep water increases with the deep water circulation: ca. 0.23 in the North Atlantic Ocean, ca. 0.30 in the Indian and Southern Ocean, ca. 0.31 in the equatorial Pacific Ocean, and ca. 0.35 in the North Pacific Ocean (Abe, 2001; de Baar, Saager, Nolting, & van der Meer, 1994; Löscher, van der Meer, de Baar, Saager, & de Jong, 1997; Quay et al., 2015). It was also proposed that the variations in the dCd/PO_4 ratio of deep water are associated with the different ballast of sinking biogenic particles: the Cd/PO_4 ratio of the silica ballast in the North Pacific is presumed to be higher than that of the $CaCO_3$ ballast in the North Atlantic (Wu & Roshan, 2015).

The concentration variations of dissolved metals (dMs), dMs/nutrient ratios, and the relationships between dMs and major nutrients among different ocean basins cannot be fully interpreted based only on biogeochemical cycles. For instance, the vertical distribution of dCd has been found highly similar to that of PO_4, exhibiting a linear relationship over the global ocean (Boyle, Sclater, & Edmond, 1976; Bruland, 1980; Roshan & Wu, 2015a; Zhang, Jensen, Fitzsimmons, Sherrell, & John, 2019). A slope change, denoted as a "kink," was observed in the North Atlantic upper water with $PO_4 < 1.3$ μmol/kg and in the South Atlantic and Pacific upper waters with $PO_4 > 1.3$ μmol/kg (Boyle, 1988). Furthermore, the linear relationship in deep waters indicates the dominant effects of water mass mixing on the distribution of dCd in the North Atlantic (Quay et al., 2015), the South Atlantic (Xie et al., 2015), and the Southern Oceans (Baars, Abouchami, Galer, Boye, & Croot, 2014). This explanation, however, could not completely elucidate the relatively low surface slope in the surface-to-subsurface water. Elderfield and Rickaby (Elderfield & Rickaby, 2000) proposed a preferential uptake of Cd over PO_4 by phytoplankton in the surface water, especially under iron-limited conditions in high-nutrient, low-chlorophyll (HNLC) areas (Cullen, 2006; Quay et al., 2015). The dCd vs. PO_4 regression line in the North Pacific is linear throughout the water column, being thus different from that observed in other oceans (Bruland, 1980; de Baar et al., 1994). A decoupling of dCd and PO_4 revealing a relative depletion of dCd was also observed in the oxygen minimum zone (OMZ) in the Northeast Pacific and North Atlantic Ocean (Janssen et al., 2014), where suspended particles were enriched with lighter isotopes of Cd (Conway & John, 2015). The authors interpreted these results by precipitation of CdS in an euxinic microenvironment around sinking particles. However, Wu and Roshan (Wu & Roshan, 2015) did not observe a relative dCd depletion in the sectional distribution of dCd/PO_4 in the OMZ in the North Atlantic, but a dCd depletion relative to PO_4 in the dCd vs. PO_4 plot. The observed depletion was ascribed to a low dCd/PO_4 ratio in shallow seawater and an enhanced regeneration of the low dCd/PO_4 ratio in the OMZ.

Dissolved Zn (dZn) has a stronger correlation with $Si(OH)_4$ than PO_4 in the global ocean (Bruland, 1980; Janssen & Cullen, 2015; Kim, Obata, Nishioka, & Gamo, 2017; Wang, Archer, Bowie, & Vance, 2019). The observed $dZn/Si(OH)_4$ ratio in seawater in the Pacific and Atlantic Oceans is approximately 0.058 mmol/mol. However, Zn uptake experiments using the marine diatom *Thalassiosira pseudonana* indicated that only 1%–3% of cellular Zn was incorporated into the silica frustule and that the dissolution of the silica resulted in a regeneration ratio of 0.3–3.2×10^{-3} (Ellwood & Hunter, 2000). Thus, diatom silica is not a major mechanism to control the dZn distribution. In fact, a decoupling of the dZn vs. $Si(OH)_4$ relationship occurs, whereas

the plot is upwards curved through the global ocean (Janssen & Cullen, 2015; Vance, de Souza, Zhao, Cullen, & Lohan, 2019; Vance et al., 2017). Janssen and Cullen (Janssen & Cullen, 2015) proposed that the plot of Zn vs. $Si(OH)_4$ in the eastern North Pacific Ocean is divided in the oxygenated upper waters and the relatively low oxygen deep waters, which could be ascribed to the preferential removal of ZnS. In contrast, Vance and co-authors (Vance et al., 2019) proposed that the preferential regeneration of Zn in a shallow water and the preferential dissolution of silica in deep water could lead to this distribution. In addition, it was suggested that the physical ocean circulation from the Southern Ocean plays an important role in the distribution of dZn (Vance et al., 2017). Moreover, it has been suggested that the scavenging of nutrient-type metals in deep water is negligible (Elderfield, 2003). However, recently, the crucial role of the reversible Zn scavenging on sinking particles was demonstrated by model calculations (Weber, John, Tagliabue, & DeVries, 2018).

Boyle and co-authors (Boyle, Sclater, & Edmond, 1977) reported full-depth profiles of Cu using unfiltered seawaters with a surface maximum of approximately 3 nmol/kg and a monotonic increase to the bottom in the central North Pacific Ocean. They also suggested that this unique distribution is maintained by the aeolian input to the surface waters, the ubiquitous scavenging in the subsurface and deep water, and a strong bottom source. In contrast, the linear distribution of dCu with depth was explained by the reversible scavenging between dissolved (d) and suspended particulate species (Little, Vance, Siddall, & Gasson, 2013). A sediment trap experiment in the North Pacific Ocean revealed that around 65% of the total Cu flux in the deepest trap was derived from primary flux from the upper water, resuspension, and hydrothermal inputs, whereas the source of the remaining 35% of the total Cu was not clarified and was mentioned as a residual flux input, implying the coexistence of alternative processes (Fischer, Dymond, Lyle, Soutar, & Rau, 1986). The authors attributed this residual to the lateral transport of particles or the re-adsorption of dCu released from bottom sediments. A recently developed box model, based on the isotope ratio and concentration of dCu, confirmed the release of dCu from the upper layer of sediments during early diagenesis (Takano, Tanimizu, Hirata, & Sohrin, 2014).

The interaction of dMs with particles in seawater has been suggested as a major control factor of the trace metal distribution in the global ocean (Goldberg, 1954; Sherrell & Boyle, 1992). Hence, a series of recent studies have focused on the role of Zn and Cu scavenging (John & Conway, 2014; Little et al., 2013; Weber et al., 2018). The suspended particulate Cd at VERTEX-IV (28°N, 155°W) decreased rapidly with depth from 2.5 to 0.2 pmol/kg, whereas the concentration of Zn was about 10 times higher than that of Cd (Bruland et al., 1994). Besides, the concentrations of the suspended particulate Cd and Zn were enriched in the North Pacific Ocean compared with those in the North Atlantic Ocean, suggesting the enhanced association of dMs with particles (Bruland et al., 1994; Sherrell & Boyle, 1992). Sediment trap experiments demonstrated that the Cd flux increases with the total particulate flux, whereas that of Ni and Cu decreases (Noriki & Tsunogai, 1992). The observed findings were attributed to the different carrier particles. Namely, it was suggested that Ni and Cu are transferred by non-biogenic inorganic and biogenic particles, whereas Cd is almost completely transferred from the latter. However, there are only limited data on the four nutrient-type metal concentrations in suspended and sinking particles in the Pacific Ocean (Bruland et al., 1994; Janssen, Abouchami, Galer, Purdon, & Cullen, 2019; Noriki & Tsunogai, 1992; Yang, Zhang, Sohrin, & Ho, 2018).

The concurrent and basin scale sectional distributions of Cd, Ni, Zn, and Cu in the North Pacific

Ocean have not been reported yet. We observed the distributions of total dissolvable (td) and d species of aluminum (Al), manganese (Mn), iron (Fe), cobalt (Co), Ni, Cu, Zn, Cd, and lead (Pb) during three GEOTRACES Japan cruises, using a multi-element analytical method (Minami et al., 2015) without ultraviolet (UV) irradiation. The difference between the td and d concentrations was defined as the labile particulate (lp) concentration. The data regarding the distribution of Al, Mn, Fe, Co, and Pb have been previously reported (Zheng et al., 2019; Zheng & Sohrin, 2019). Herein, we report a comprehensive dataset of td, d, and lp species of the nutrient-type trace metals (Cd, Ni, Zn, and Cu) to elucidate the major factors that control their distribution and their correlation with the major nutrients PO_4 and $Si(OH)_4$. The data that refer to the other metals are also used for the discussion of the current findings. The simultaneous observation of the trace metals will help to improve our understanding of scavenging and other processes relative to the nutrient-type trace metals.

2 Materials and Methods

2.1 Materials and sampling

Clean seawater samples were collected during three GEOTRACES cruises of R/V Hakuho Maru; KH-05-2 (Aug–Sep 2005), KH-11-7 (Jul 2011), and KH-12-4 (Aug–Sep 2012) (Figure 1). The details of the used materials and the sampling process have been reported in previous studies (Zheng et al., 2019; Zheng & Sohrin, 2019). The KH-11-7 and KH-12-4 cruises were formal studies of GEOTRACES Japan, which occupied the GEOTRACES sections of GP18 (165°E) and GP02 (47°N). The samples used to estimate the total dissolved trace metals (tdMs) were acidified to pH 2.2 with ultrapure HCl (Tamapure AA-10, Tama Chemicals) immediately after collection. A portion of the seawater samples was collected and filtered on board using 0.2 μm filters to acquire the dMs samples. Nuclepore polycarbonate membrane filters (Whatman) were used for KH-05-2 and KH-11-7, whereas for KH-12-4, AcroPak capsule filters (Pall) were applied. The filtered seawater samples were also acidified to pH 2.2 with ultrapure HCl and stored at room temperature for at least 1 year prior to analysis. The Ocean Data View software

was applied for the data analysis and the preparation of the figures (Schlitzer, 2015).

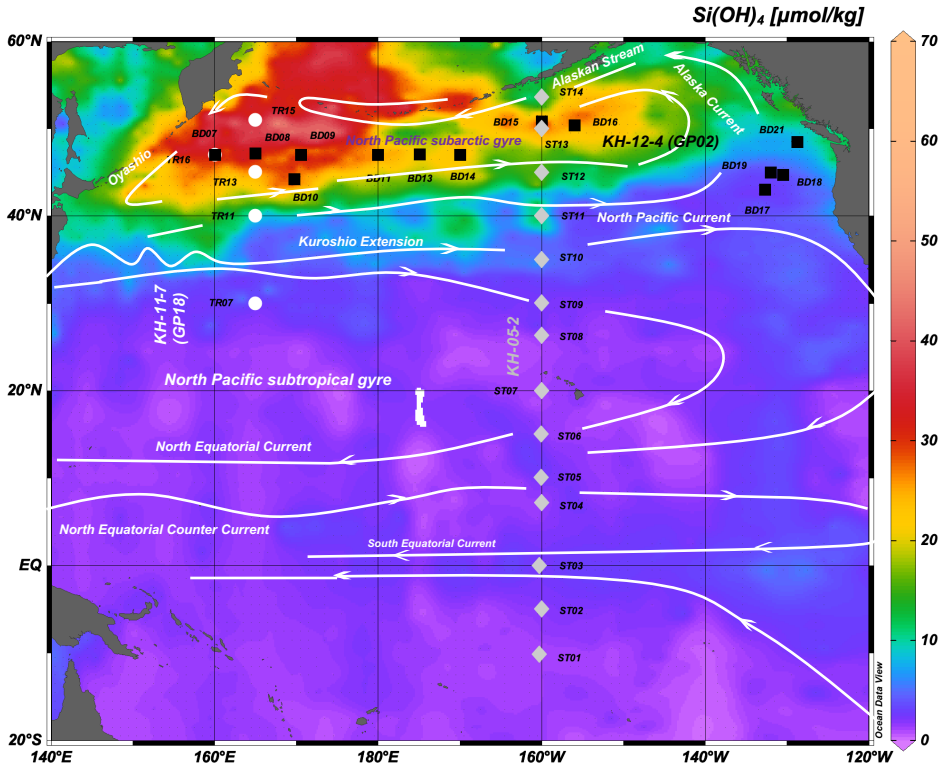

Figure 1. Map of the study area and the sampling stations in the North Pacific Ocean. White solid lines indicate the surface currents. The background color represents the annually averaged surface $Si(OH)_4$ concentrations obtained in 2018 (www.nodc.noaa.gov).

2.2 Analytical methods

An offline automated solid-phase extraction system (SPE-100, Hiranuma Sangyo) with a column of Nobias Chelate-PA1 resin (Hitachi High-Technologies) was used to preconcentrate the trace metals (Al, Mn, Fe, Co, Ni, Cu, Zn, Cd, and Pb) in seawater (Minami et al., 2015). The applied analytical methods were presented in our previous studies in detail (Zheng et al., 2019; Zheng & Sohrin, 2019). The collected seawater samples were adjusted to pH 6.00 ± 0.05 in a clean room (class 1000) and immediately introduced to the SPE-100 system. Procedural blanks were measured using ultrapure water between the analyses of the seawater samples. A high-resolution inductively coupled plasma mass spectrometer (HR-ICP-MS, Element 2, Thermo Fisher Scientific) was used to determine the concentrations of the investigated trace metals by the calibration curve method. The detection limits (*DL*) for the tdMs and dMs samples were calculated as three times the standard deviation (sd) of the procedural blank, whereas those for lpMs were defined using the equation $\mathbf{2} \times \sqrt{\mathbf{2}} \times \mathbf{0.05} \times \boldsymbol{C}_{\mathrm{ave}}$, considering the propagation of uncertainty, where C_{ave} represented the average concentration of dMs. The procedural blanks and the *DL* for all the species are summarized in Table S1.

A series of certified reference materials for trace metals CASS-5, 6 and NASS-6, 7 and the

GEOTRACES open-ocean reference samples GS, GD, GSP, and GSC were measured to ensure the accuracy of the applied method (Table S2). The concentrations found for Ni, Zn, and Cd were in good agreement with the certified and/or consensus values, whereas the Cu concentrations were in line with the certified values of CASS and NASS, which were gamma irradiated. In contrast, the Cu concentrations were slightly lower than the consensus values of the GEOTRACES reference samples. The consensus values were obtained after UV irradiation, whereas the current samples were not subjected to UV irradiation, meaning that a portion of dCu that forms strong complexes with organic ligands might not be measured. Given that the application of UV irradiation led to unexpected contamination of some metals (Zheng et al., 2019) and that the data obtained for Cu in the current study were sufficiently reproducible, UV irradiation was not applied in this study.

2.3 Cross-over stations

Cross-over stations stipulated by GEOTRACES provide a measure of data consistency (http://www.geotraces.org). Stations TR16 from KH-11-7 and BD07 from KH-12-4 are located at the same position and serve as internal cross-over stations in this study. The vertical profiles of tdMs, dMs, $Si(OH)_4$, PO_4, and nitrate (NO_3) fit well between TR16 and BD07 within analytical uncertainty (Figure S1). Although all the regression lines have coefficients of determination (r^2) higher than 0.89 (Figure S2), they have positive intercepts. Moreover, the surface water at BD07 has lower salinity, higher temperature, and lower $Si(OH)_4$ and PO_4 concentrations than TR16, suggesting the higher influence of the Kuroshio Waters. Our data indicate also that the concentrations of tdMs and dMs are lower in the Kuroshio Waters.

Stations ST13, ST14 of the KH-05-2 cruise are located 100 km south and 300 km north of the station BD15 of KH-12-4, respectively. The vertical profiles of tdMs, dMs, $Si(OH)_4$, PO_4, and NO_3 fit well among ST13, ST14, and BD15 within analytical uncertainty (Figure S3). All the regression lines between ST13 and BD15 have r^2 values higher than 0.96 (Figure S4). The Ni, Cd, $Si(OH)_4$, and PO_4 concentrations in the surface water are lower at BD15 compared with ST13, possibly due to the higher chlorophyll *a* (Chl. *a*) content that allowed for a higher Ni, Cd, and nutrient uptake. In previous papers, we reported that the concentrations of Al, Mn, and Fe substantially decrease from ST14 to ST13 due to boundary scavenging (Zheng et al., 2019; Zheng & Sohrin, 2019). Nevertheless, the data in this work do not reveal that boundary scavenging significantly affects the distribution of nutrients and the nutrient-type trace metals. Only Cu exhibits a surface maximum at ST14, where the Alaskan Stream flows and the surface maxima of Mn and Co occur (Zheng et al., 2019). In conclusion, it is indicated that the analytical precision of tdMs and dMs is comparable to that of nutrients.

3 Results

3.1. Hydrography

Figure 1 presents the sampling stations of this study with the annually averaged surface $Si(OH)_4$ concentrations as obtained in 2018 (www.nodc.noaa.gov). The white solid lines indicate the surface currents. The Oyashio Current, the North Pacific Current, the Alaska Current, and the Alaskan Stream form the anticlockwise upwelling North Pacific subarctic gyre to the north of 40°N. The North Pacific subtropical gyre to the south of the Subarctic Front consists of the

Kuroshio Extension, the North Pacific Current, and the North Equatorial Current (Yuan & Talley, 1996).

There are three major water masses at the intermediate depth in the North Pacific Ocean: the North Pacific Intermediate Water (NPIW), the Antarctic Intermediate Water (AAIW), and the Equatorial Pacific Intermediate Water (EqPIW). NPIW originates from the Okhotsk Sea Mode Water and is formed to the east of Hokkaido, Japan, and spreads to the southeast (Talley, 1993). NPIW is characterized by low salinity and low density with a potential density anomaly (σ_θ) of 26.4–27.2 (average: 26.8) (Yasuda, 1997). AAIW originates from the north of the Subantarctic Front (Bostock, Opdyke, & Williams, 2010; Talley, Pickard, Emery, & Swift, 2011) and extends to ca. 15°N in the tropical–subtropical transition (Talley et al., 2011). EqPIW is formed by a combination of AAIW and the Pacific Deep Water (PDW). Among the three water masses, NPIW is the shallowest (200–800 m in depth), followed by EqPIW (700–1000 m in depth) and AAIW (600–1100 m in depth) (Bostock et al., 2010; Talley et al., 2011).

Two distinct deep waters exist in the North Pacific Ocean: the Circumpolar Deep Water (CDW) and the PDW. The upper CDW (UCDW) and the lower CDW (LCDW) are two branches of CDW that are formed by mixing the North Atlantic Deep Water and other deep waters in the Southern Ocean. PDW is formed internally in the North Pacific by mixing upwelled bottom waters with the UCDW. PDW and UCDW appear in almost the same density range, whereas UCDW flows northwards and PDW southwards (Talley et al., 2011). LCDW flows at the deepest depth into the Pacific Ocean and is characterized by high salinity (S = 34.72).

3.2 Distributions

All the data for tdMs, dMs, lpMs, nutrients, and oceanographic properties are listed in Table S3. The statistical summary of tdMs, dMs, and lpMs is presented in Table S4. lpCd, lpNi, and lpZn are not further discussed, because they were detected in only a few of the samples collected near the continents. The concentrations of dZn and tdZn collected from the KH-05-2 cruise were removed from the dataset because of their contamination from the sacrificial Zn electrode that was attached to the seawater sampling system. Not detected (ND) data below the *DL* were assigned to a value of $\boldsymbol{DL \times (1/\sqrt{2})}$ (Croghan & Egeghy, 2003) for further analysis and the preparation of the corresponding figures.

The full-depth sectional distributions of $Si(OH)_4$, PO_4, NO_3, the apparent oxygen utilization (AOU), dCd, dNi, dZn, and dCu at 160°W, 165°E, and 47°N are presented in Figures 2, S5, and 3, respectively. The concentration of $Si(OH)_4$ in the surface water is 25 μmol/kg in the western subarctic gyre and almost zero in the subtropical gyre and around the Juan de Fuca Ridge (JdFR) (Figure S6). The surface concentration of PO_4 and NO_3 in the subarctic gyre, which is known as one of the HNLC regions, exceeds 0.5 and 7 μmol/kg, respectively. The surface concentrations of major nutrients at ST14 are extremely low, where Chl. *a* reaches the maximum of 2.7 μg/kg. $Si(OH)_4$, PO_4, NO_3, and AOU generally increase with depth and latitude. PO_4, NO_3, and AOU exhibit maximum concentrations in a depth range of 1000–2000 m (Figures 2, 3, S5). In contrast, $Si(OH)_4$ increases along the flow of LCDW in the North Pacific Ocean and exhibits a maximum

in the depth range of 1500–5000 m at 30–40°N.

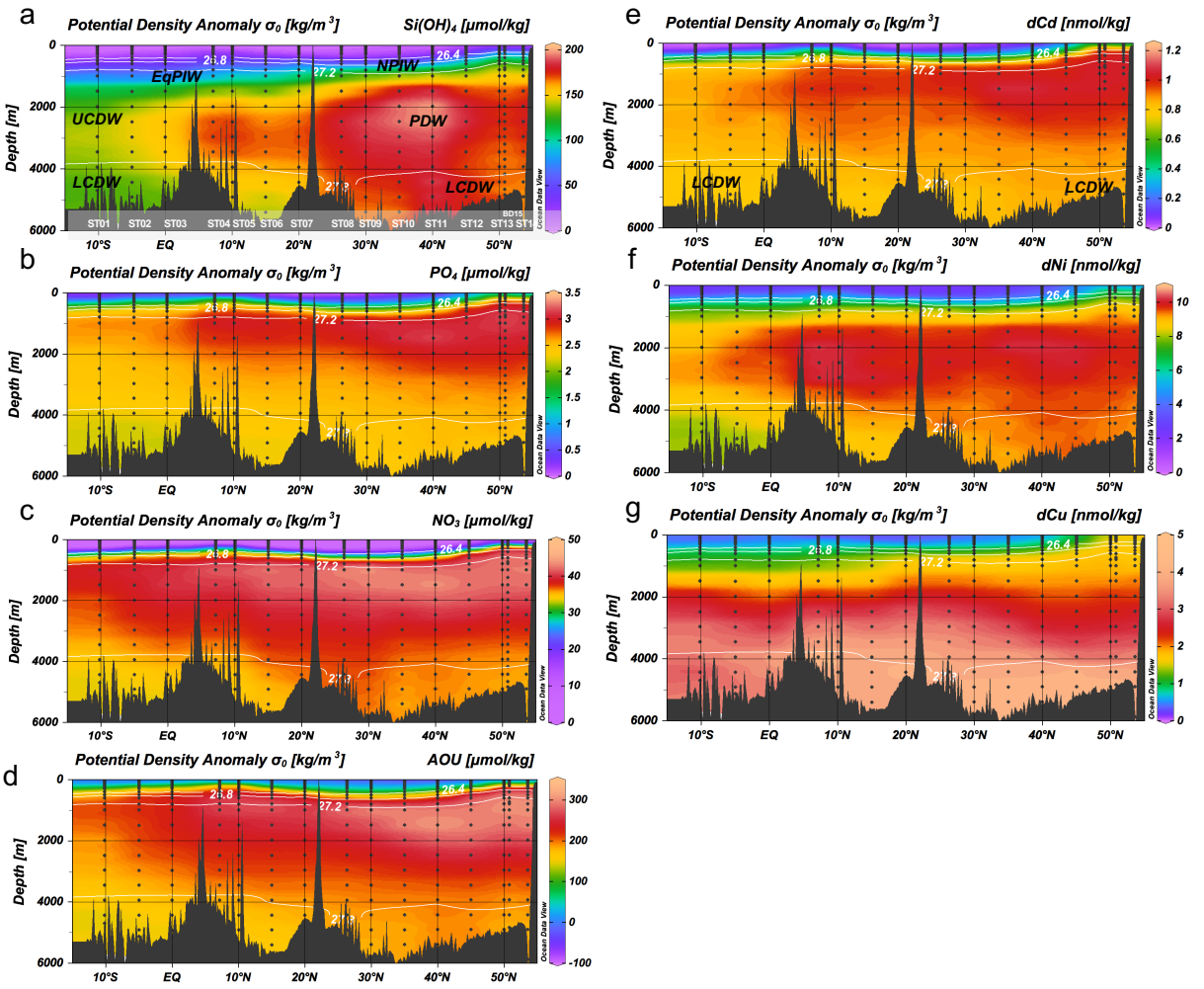

Figure 2. Full-depth sectional distribution of (a) silicate [$Si(OH)_4$], (b) phosphate (PO_4), (c) nitrate (NO_3), (d) apparent oxygen utilization (AOU), (e) dCd, (f) dNi, and (g) dCu at 160°W. The white solid lines indicate potential density anomalies. NPIW: North Pacific Intermediate Water; EqPIW: Equatorial Pacific Intermediate Water; UCDW: Upper Circumpolar Deep Water; LCDW: Lower Circumpolar Deep Water; PDW: Pacific Deep Water.

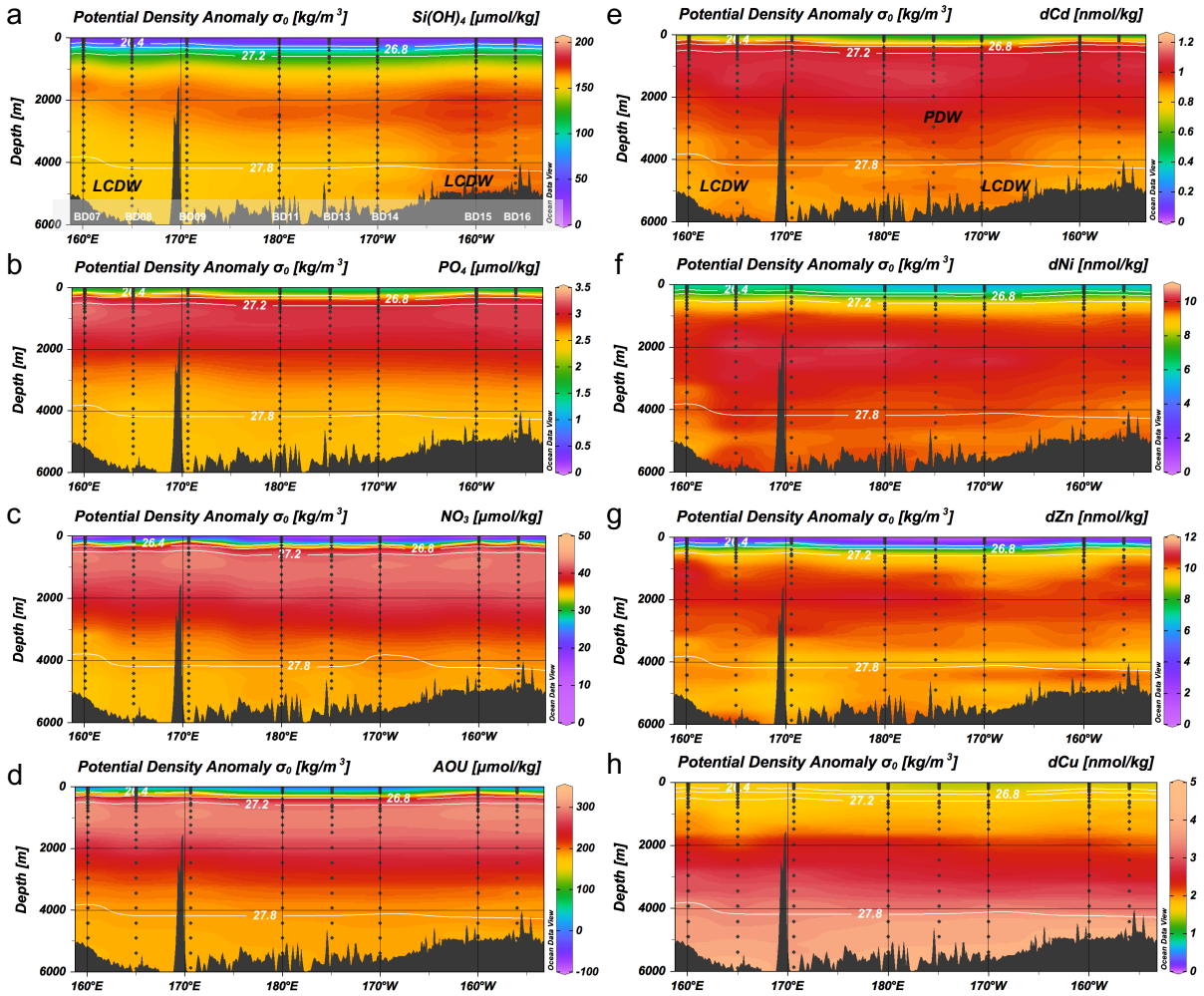

Figure 3. Full-depth sectional distribution of (a) $Si(OH)_4$, (b) PO_4, (c) NO_3, (d) AOU, (e) dCd, (f) dNi, (g) dZn, and (h) dCu at 47°N (GP02). The white solid lines indicate potential density anomalies.

Based on Figures 2, 3, and S5, dCd is sectionally distributed similarly to PO_4 and NO_3. In addition, the horizontal distribution of dCd reveals the existence of sources around the northern continents like those of $Si(OH)_4$, PO_4, and NO_3 (Figure S6). dCd exhibits correlation coefficients (r) higher than 0.98 with both PO_4 and NO_3. However, dCd has a unique maximum at a 200 m depth (σ_θ = 27.0) at the subarctic stations (Figures S1, S3). The concentration of dCd is extremely low in the surface water south to 40°N, whereas it reaches the maximum of 1.22 nmol/kg at a depth of 200 m (47.0°N, 170.6°E). The maximum depth of dCd increases from 200 to 800 m with the latitude decreasing from 47°N to 10°S. Moreover, lpCd is usually lower than the *DL* of 0.11 nmol/kg, which is consistent with the previously reported low concentrations of particulate Cd (0.05–38 pmol/kg) in the North Pacific (Bruland et al., 1994; Janssen et al., 2019). lpCd reaches a value of 0.16 nmol/kg in the surface layer at the station ST14, where the Chl. *a* maximum occurs, and it is 0.24 nmol/kg at a 200 m depth at the station TR15, which is close to the Kamchatka Peninsula.

The sectional distributions of dNi resemble those of $Si(OH)_4$, PO_4, and NO_3 (Figures 2, 3, S5).

The dNi profiles exhibit the lowest concentrations (2.3–5.9 nmol/kg) in surface water, a broad maximum of 10.5 nmol/kg at a 1500–3000 m depth, and a slight decrease above the bottom. The horizontal distribution of dNi indicates the presence of sources around the northern continents like those of $Si(OH)_4$, PO_4, NO_3, and dCd (Figure S6). The correlation coefficients between dNi and the major nutrients are >0.91.

Similarly to dNi, the sectional distributions of dZn resemble those of $Si(OH)_4$, PO_4, and NO_3 (Figures 3, S5). The broad maximum of dZn occurs at a depth of 1000–2000 m, which is deeper than the maximum of dCd. At the northern stations, a maximum of dZn appears at a depth of approximately 200 m, like that of dCd (Figures S1, S2). In contrast to dCd, dNi, and major nutrients, dZn in surface water sharply decreases with the distance from the stations TR16/BD07 near the Kuril–Kamchatka Trench to the eastern stations in the western subarctic gyre (Figure S6). The correlation coefficients between dZn and the major nutrients are >0.91 similarly with dNi.

Unlike Cd, Ni, and Zn, the sectional distributions of dCu are apparently not similar to those of the major nutrients and AOU (Figures 2, 3, S5). dCu has low concentrations in the surface water except the stations around JdFR and near the Aleutian Islands (Figure S6). The surface concentration of dCu is the highest at ST14, whereas that of dCd, dNi, and dZn is low compared with the surrounding stations (Figure S6). dCu increases linearly until a depth of 3000 m is reached. At stations south to 40°N and at depths of 3000–4000 m, dCu exhibits a maximum of 2.7–4.4 nmol/kg, which remains relatively constant or slightly decreases below this depth. In contrast, at stations north to 40°N and at the same depth, dCu has a lower concentration (2.4–3.1 nmol/kg), which generally increases to the bottom. On a surface of 4500 m depth, dCu has a uniformly high concentration in the Northeast Pacific Basin (Figure S6). Among the four metals, only lpCu is detected in 50% of the samples, indicating a significant contribution of the suspended particulate matters to the Cu distribution. The sectional distribution of lpCu is presented in Figure 4. lpCu generally increases with depth, and the highest concentration (1.37 nmol/kg) is achieved in abyssal seawater near the Kuril–Kamchatka Trench. Moreover, the lpCu/tdCu ratio for all the data is 0.18 ± 0.12 (average ± standard deviation) and is as high as the

lpM/tdM ratios (ca. 0.2) observed for Mn and Co (Zheng et al., 2019).

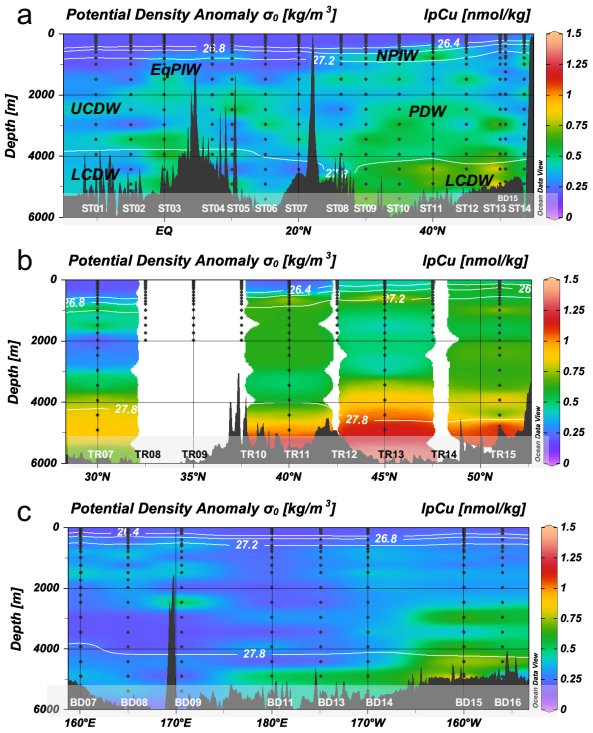

Figure 4. Full-depth sectional distribution of lpCu at (a) 160°W, (b) 165°E, and (c) 47°N. The white solid lines indicate potential density anomalies.

4. Discussion

4.1 Biogeochemical control on the distribution of Cd

4.1.1 Cd vs. PO_4

The dCd vs. PO_4 plot exhibits a linear relationship for all the data (Figure 5a).

334 dCd [nmol/kg] = 0.360 × PO_4 [µmol/kg] – 0.058 $r^2 = 0.971$, $n = 605$.

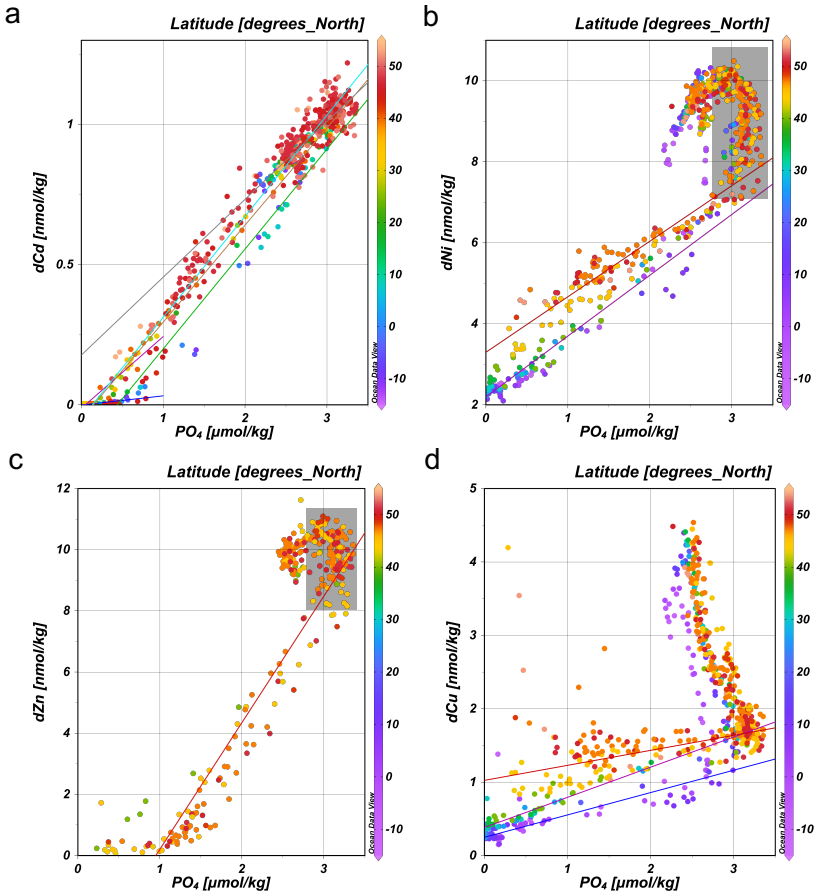

335 Figure 5. Plots of (a) dCd vs. PO_4, (b) dNi vs. PO_4, (c) dZn vs. PO_4, and (d) dCu vs. PO_4. The
336 plot color indicates the latitude and the color lines indicate the different regression lines, which
337 are summarized in Table 1. The gray shadow indicates the plot area, where dZn and dNi increase
338 independently of PO_4.

339 The slope of 0.360 is in the range of the Cd/P ratio that is observed in phytoplankton (0.20–0.56
340 mmol/mol) (Collier & Edmond, 1984; Ho, Wen, You, & Lee, 2007; Ho et al., 2009). However,
341 the dCd vs. PO_4 plot at each station significantly varies in the North Pacific Ocean. The data
342 points generally upshift with the latitude. The regression lines for the typical groups are listed in
343 Table 1. To the south of 20°N, the points from the upper 800 m are divided into two parts,
344 whereas the dCd/PO_4 slope is 0.0328 for 0–100 m and 0.356 for 100–800 m, resulting in a kink,
345 which is formed at a lower PO_4 concentration (0.5 µmol/kg) than that observed in other oceans
346 (Baars et al., 2014; Boyle, 1988; Frew & Hunter, 1992, 1995). By moving to the north in the
347 North Pacific Ocean, the kink disappears except the stations around JdFR. The concentration of
348 dCd is less than the *DL* down to 150 m at ST01. The depth of depletion in dCd becomes
349 shallower at northern stations and is 50 m at ST11 (40°N). To the north of 40°N, the surface
350 concentration of dCd becomes higher than the *DL*. Probably, the disappearance of the kink in the
351 subarctic North Pacific Ocean is a consequence of supply of dCd to the surface water from the
352 northern continents. The data points for deep waters (>800 m) in the whole North Pacific Ocean
353 converge on a single line with a slope of 0.278. This could be attributed to the mixing, which is

the major factor to determine the dCd concentration in deep waters.

4.1.2 The effect of regeneration and water circulation on the dCd distribution

The fractionation factor (*FF*) is defined to investigate the preferential uptake of dCd over PO_4 based on the following equation (Elderfield & Rickaby, 2000; Quay et al., 2015):

$$FF(\mathrm{dCd}) = (\mathrm{Cd{:}PO_{4,\ particles}})/(\mathrm{dCd/PO_{4,\ seawater}})$$

where the $Cd{:}PO_{4,\ particles}$ ratio is estimated by the dCd vs. PO_4 slope in nutricline, because the slope represents the regeneration ratio from biogenic particles. The nutricline depth is defined as the shallowest depth where the nutrient concentration exceeds the mixed layer value of 0.5 μmol/kg for $Si(OH)_4$ and 0.05 μmol/kg for PO_4 (Laanemets, Kononen, Pavelson, & Poutanen, 2004). The *FF*(dCd) in this study varies from 0.7 at northern stations to 44.9 at southern stations with an average of 9.3 ± 13.6 (Figure 6a), which is much higher and more scattered than the reported value of 1.8 ± 1.0 in the North Pacific (Quay et al., 2015). Moreover, the *FF*(dCd) is extremely high at stations to the south of 20°N and around JdFR, where a kink appears on the dCd vs. PO_4 plot. The strong depletion of dCd is probably the results of the preferential uptake of dCd by phytoplankton at these stations. High contents of dCd in the surface water and low *FF*(dCd) values are observed at the stations to the north of 20°N and especially to the north of 40°N, indicating that the preferential uptake of dCd is not an important factor at these stations.

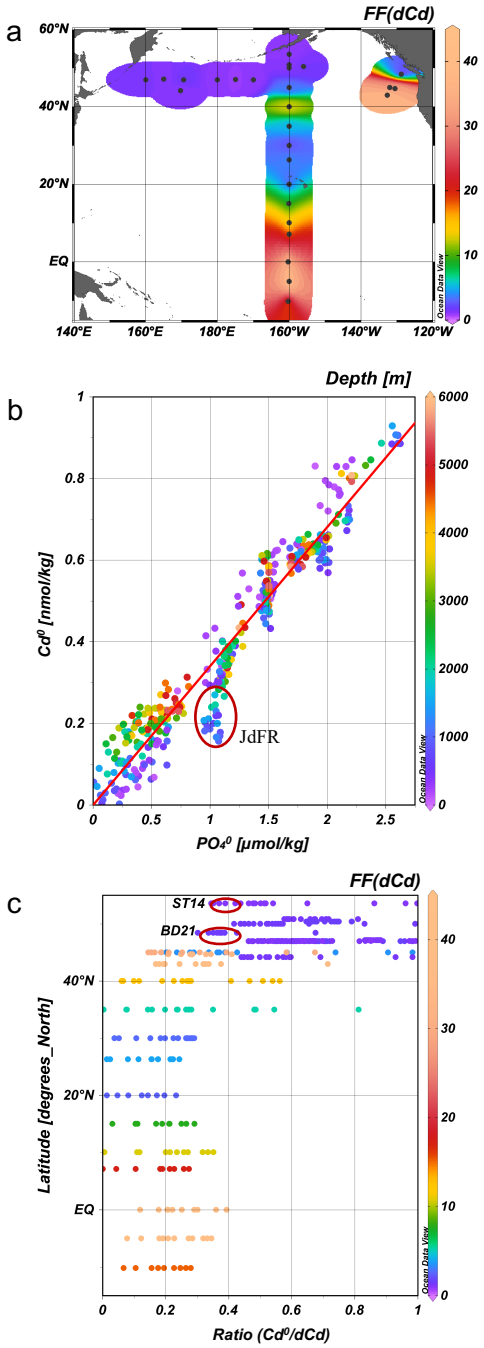

371 Figure 6. (a) Horizontal distribution of the Cd fractionation factor (*FF*). (b) preformed Cd (Cd^0)
372 vs. preformed phosphate (PO_4^0) plot. The red circle indicates data obtained from JdFR. (c)
373 Latitude vs. Cd^0/dCd. The red circles indicate the data obtained from water at a depth of 500–
374 2500 m at stations ST14 and BD21. The plot color in (b) denotes the depth, and that in (c)
375 denotes the *FF*(dCd).

376 The preformed nutrient concentration has been used as a tracer for water masses because of their
377 conservative nature (Sarmiento & Gruber, 2006). Redfield et al. established the respiratory
378 equation of the average phytoplankton and indicated that the ratio of dissolved PO_4 and O_2 is

1:138 (Redfield, Ketchum, & Richards, 1963). Thus, the preformed phosphate (PO_4^0) can be defined as follows (Emerson & Hedges, 2008; Kudo, Kokubun, & Matsunaga, 1996):

$$PO_4^0\ [\mu mol/kg] = PO_4 - AOU/138$$

In this study, we used the slope of PO_4 vs. AOU in the upper 800 m instead of the Redfield ratio, whereas the data of AOU < 0 in surface water were removed from the calculation. Assuming that the Redfield ratio can be extended to dCd (Kudo et al., 1996), the preformed dCd (Cd^0) is defined as follows:

$$Cd^0\ [nmol/kg] = dCd - AOU \times (a \times b)$$

where a and b denote the ratio of Cd:PO_4 and PO_4:AOU using the data in the upper 800 m, respectively. The Cd^0 data that are lower than zero are not included in the discussion. The plots of Cd^0 vs. PO_4^0 have a strong linear relationship with an intercept of almost zero (Figure 6b):

$$Cd^0\ [nmol/kg] = 0.341 \times PO_4^0 - 0.000 \qquad r^2 = 0.931,\ n = 379.$$

The zero intercept indicates that the Cd^0/PO_4^0 ratio is constant among the water masses. Moreover, the slope of 0.341 is equal to the observed Cd/PO_4 ratio in deep water. This linearity also supports the dominant effect of biogeochemical cycling on the distribution of dCd. In addition, plots deviate from the regression line are marked in a red circle in Figure 6b, which represent data from JdFR. This is probably due to removal of CdS near hydrothermal vents.

The distribution of Cd^0/dCd against the latitude is presented in Figure 6c, where the plot color indicates the *FF*(dCd). The plot demonstrates that the stations to the south of 35°N have *FF*(dCd) > 2.4 and Cd^0/dCd < 0.4, whereas the stations to the north of 45°N generally have *FF*(dCd) < 1.6 and Cd^0/dCd > 0.4. Thus, the regeneration is proven important for stations south to 35°N. As an exception, the samples collected from depths ranging between 500 and 2500 m at ST14 and BD21 have low Cd^0/dCd ratios (plots in red circles). These stations are nearest to the continent, implying that apart from the mixing of water masses, the supply from the northern continents may also be important.

4.2 Effects of water circulation, scavenging, and remineralization on the distribution of Cu, Ni, and Zn

4.2.1 Water circulation: dMs vs. $Si(OH)_4$

The correlation of Cu and $Si(OH)_4$ in the ocean has been studied since the 1980s (Monteiro & Orren, 1985; Roshan & Wu, 2015b; Saager, De Baar, & Howland, 1992). As presented in Figure 7, dCu has a strong correlation with $Si(OH)_4$ from surface to bottom in both the North and South Atlantic Oceans. In the North Atlantic Ocean, dCu is calculated as dCu [nmol/kg] = 0.0351 × $Si(OH)_4$ [μmol/kg] + 0.81 (r^2 = 0.772, for full depth) (Roshan & Wu, 2015b). In contrast, a linear relationship is observed at a depth < 1500 m in the Southern Ocean, where dCu is estimated as dCu [nmol/kg] = 0.0121 × $Si(OH)_4$ [μmol/kg] + 0.74 (r^2 = 0.701) (Heller & Croot, 2015; Schlitzer et al., 2018). The plots in waters deeper than 1500 m slightly curve upwards from the regression line. In the South Pacific Ocean, a linear relationship is also observed above a 1500 m depth, where dCu [nmol/kg] = 0.0142 × $Si(OH)_4$ [μmol/kg] + 0.50 (r^2 = 0.943) (Roshan

& Wu, 2018). Thus, the increase in dCu at depths > 1500 m is stronger than that in the Southern Ocean. In this study, a more intense increase in dCu is observed at a depth of >1500 m in the North Pacific Ocean. Except the surface maximum of dCu, the regression line of Cu and $Si(OH)_4$ for depths of 20–1500 m is (Figure S7d):

$$dCu\ [nmol/kg] = 0.00773 \times Si(OH)_4\ [\mu mol/kg] + 0.76 \qquad r^2 = 0.706,\ n = 331.$$

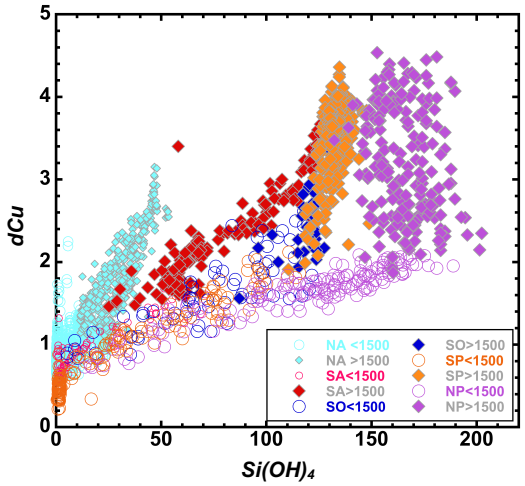

Figure 7. Compilation of global data of dCu vs. $Si(OH)_4$. NA: the North Atlantic Ocean (Jacquot & Moffett, 2015; Roshan & Wu, 2015b); SA: the South Atlantic Ocean; SO: the Southern Ocean (Heller & Croot, 2015); SP: the South Pacific Ocean (Roshan & Wu, 2018); NP: the North Pacific Ocean in this study. Some of the data are from the GEOTRACES Intermediate Data Product 2017 (Schlitzer et al., 2018).

The slope of the regression line decreases, and the accumulation of dCu over $Si(OH)_4$ in deep water increases along the route of thermohaline circulation through the global oceans. This phenomenon is probably due to the redissolution of scavenged dCu from particles and sediments, whereas the stagnant deep-water circulation in the North Pacific Ocean enhances the accumulation of dCu more than in any other oceans.

The dZn vs. $Si(OH)_4$ plot in this study depicts an upward convex with a kink at 84 µmol/kg of $Si(OH)_4$ (Figure S7c). Kim and co-authors (Kim, Obata, Kondo, Ogawa, & Gamo, 2015; Kim et al., 2017) found the same trend and attributed it to the supply of the intermediate water with a high dZn/$Si(OH)_4$ ratio. Although the dNi vs. $Si(OH)_4$ in this study exhibits a linearity throughout the water column at stations to the north of 40°N, an upward convex is also observed at stations to the south of 40°N and in a depth range of 300–2000 m (Figure S7b), indicating the effect of intermediate water (EqPIW and NPIW) and UCDW with high dNi/$Si(OH)_4$ ratio (Table S5). In contrast, dCd and $Si(OH)_4$ does not exhibit a linear relationship (Figure S7a).

4.2.2 Scavenging and remineralization: dMs/PO_4 ratios and dMs vs. PO_4

Cu, Ni, and Zn are widely utilized as co-factors of enzymes (Twining & Baines, 2013) and will be incorporated into soft tissues of organisms in a similar manner with Cd. Ellwood and Hunter (Ellwood & Hunter, 2000) have proved that only a few percentages of Zn is incorporated in the

silica frustule of a diatom, which may be also valid for Ni and Cu. The plots of dMs vs. AOU and major nutrients vs. AOU are presented in Figure S8, indicating that each dM uniquely depends on AOU.

NO_3 exhibits strong linearity with the AOU, and this pattern is similar to the PO_4 vs. AOU plot (Figure S8). NO_3 and PO_4 are mainly influenced by biogeochemical cycles and have similar vertical profiles with each other. At waters deeper than 800 m, NO_3/PO_4 decreases by 4% when the AOU is increased from 150 to 300 µmol/kg (Figure S9). The decrease of dCd/PO_4 ratio is 4%, which is comparable with that of NO_3/PO_4 (Figure 8a). In contrast, both dNi/PO_4 and dZn/PO_4 decrease by 21%, whereas dCu/PO_4 decreases by 69% (Figure 8b–8d). These results indicate that an alternative sink, namely specifically scavenging, must be important for Cu, Ni, and Zn. Otherwise, their ratios would not change with the AOU.

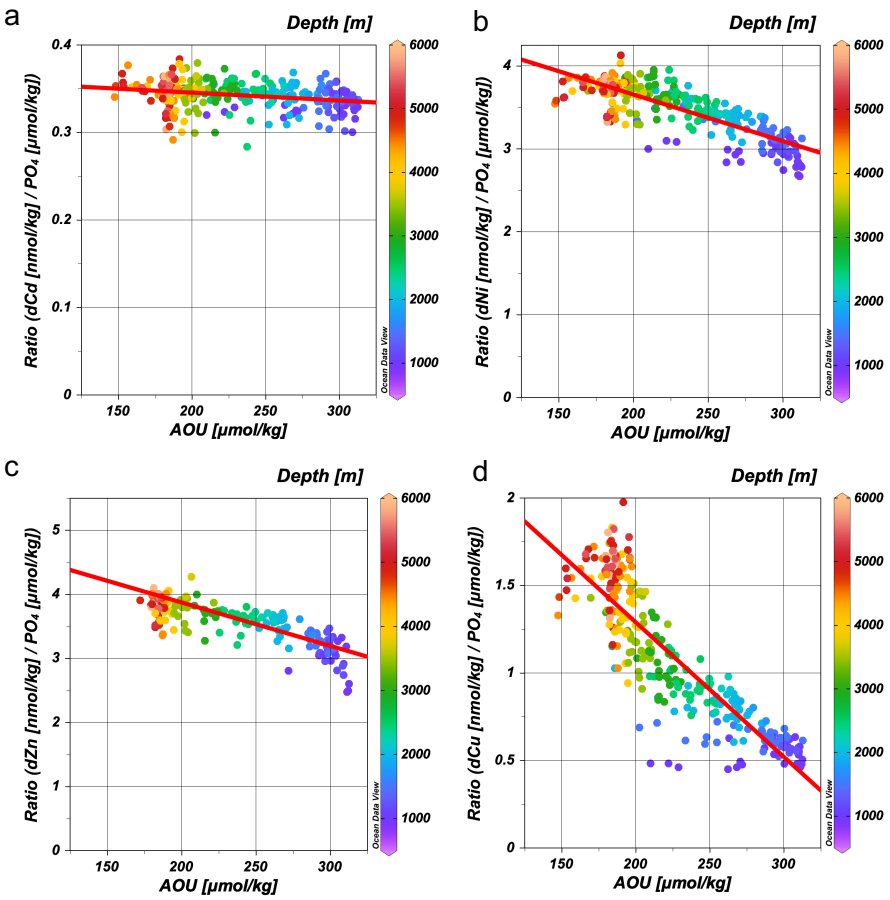

Figure 8. Plots of dMs/PO_4 ratios vs. AOU at depths > 800 m; (a) dCd/PO_4 vs. AOU, (b) dNi/PO_4 vs. AOU, (c) dZn/PO_4 vs. AOU, (d) dCu/PO_4 vs. AOU. The plot color indicates the depth.

The vertical profiles of the dMs/PO_4 ratio are presented in Figure 9, where the Ms/PO_4 ratio range in phytoplankton is shown as gray shadow (Bruland, Donat, & Hutchins, 1991; Collier & Edmond, 1984; Ho et al., 2007; Kuss & Kremling, 1999). Almost all the plots of the dCd/PO_4 ratio appear within the range of phytoplankton, indicating that the concept of the Redfield ratio can be applied to Cd as well (Figure 9a). However, those of Ni, Cu, and Zn are largely out of the

phytoplankton range. The dMs/PO_4 ratios in each water mass are listed in Table 2. The dCd/PO_4 ratio is 0.34 ± 0.02 mmol/mol (n = 296) at a depth lower than 800 m, which is consistent with the reported data (Quay et al., 2015). However, the dCd/PO_4 ratio significantly varies in the upper water. The dCd/PO_4 ratio reaches a maximum of 0.93 mmol/mol in the surface water at around 20–30°N, where PO_4 is depleted and dCd is probably supplied from the Hawaiian Islands (Figure 10a). In addition, another high Cd/PO_4 ratio is identified near the northern continental shelf and spread to around 30°N along 26.8σ_θ, where intermediate water exists. This trend is similar to that of dCo (Zheng et al., 2019).

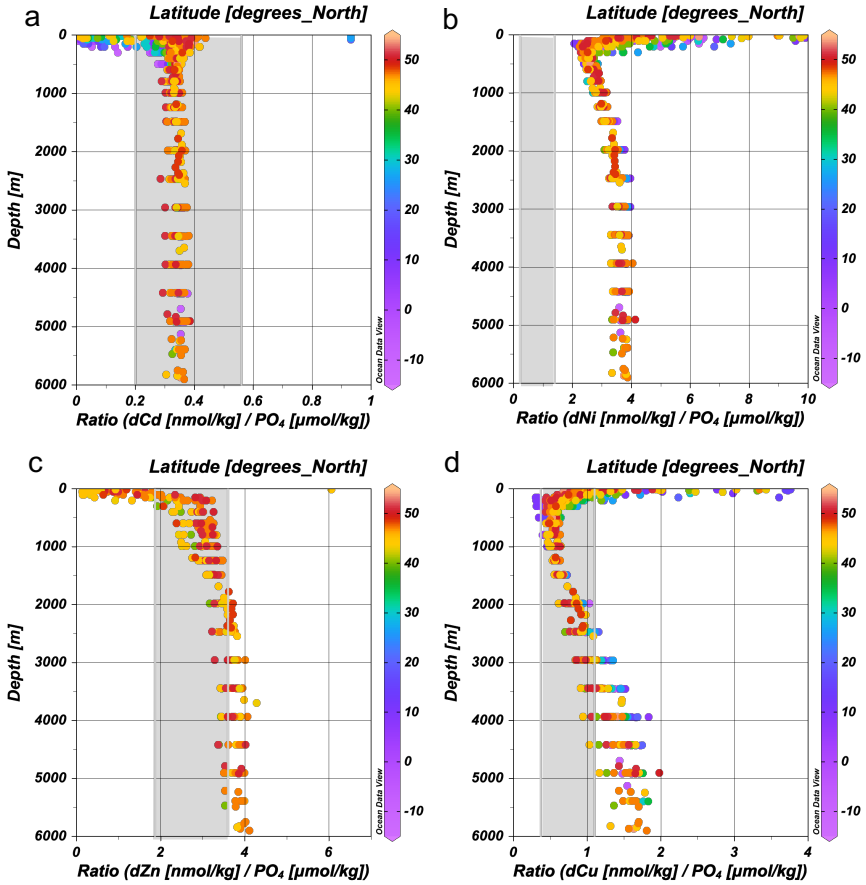

Figure 9. Depth profiles of (a) dCd/PO_4, (b) dNi/PO_4, (c) dZn/PO_4, and (d) dCu/PO_4. The x axes of (b) and (d) are expanded to show details in deep water. The gray shadows mark the range of the Ms/PO_4 ratio in phytoplankton (Bruland et al., 1991; Collier & Edmond, 1984; Ho et al., 2007; Kuss & Kremling, 1999).

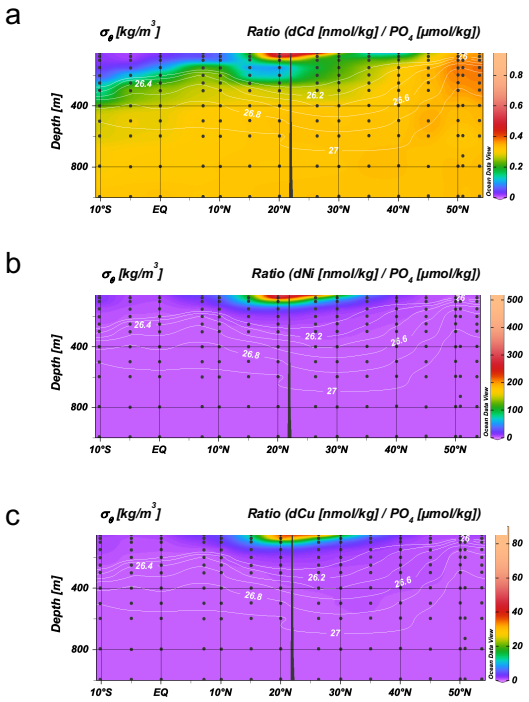

475 Figure 10. Sectional distributions of (a) dCd/PO_4, (b) dNi/PO_4, and (c) dCu/PO_4 at depths of 0–
476 1000 m at 160°W.

477 The dCu/PO_4 ratio reaches a maximum of 82 mmol/mol in the surface water at around 20–30° N
478 similarly to dCd/PO_4 (Figures 10c). The dCu/PO_4 ratio sharply decreases with depth and has a
479 minimum of 0.30 mmol/mol at depths ranging from 150 to 800 m (Figure 9d). The sharp
480 decrease in the dCu/PO_4 ratio in the subsurface water reflects the regeneration of PO_4 and the
481 scavenging of dCu. Then, the dCu/PO_4 ratio increases to the bottom, whereas many data points
482 are outside the range of the dCu/PO_4 ratio in phytoplankton. The high dCu/PO_4 ratio is due to the
483 selective accumulation of dCu in deep water through the ocean circulation and the redissolution
484 from sinking particles and bottom sediments.

485 Similarly to dCu and dCd, the dNi/PO_4 ratio in the surface water is extremely high at around 20–
486 30°N (Figure 10b). The dNi/PO_4 ratio decreases from the surface maxima to the subsurface
487 minima of 2 mmol/kg at a 200 m depth and then slightly increases to 3000 m (Figure 9b). All the
488 dNi/PO_4 ratios are higher than the Ni/PO_4 ratio in phytoplankton due to the excess dNi in
489 seawater throughout the North Pacific Ocean. The dZn/PO_4 ratio in the surface water is 0.15–1.2
490 except 6.0 at BD18 (Figure 9c). The results suggest that the preferential uptake of dZn by
491 phytoplankton is ubiquitous in the subarctic North Pacific Ocean, which is consistent with the
492 significant west-to-east gradient in the dZn concentration in the surface water (Figure S6c). The
493 dZn/PO_4 ratio increases with depth in a manner similar to dCd/PO_4 (Figures 9c, 9a). However,
494 the dZn/PO_4 ratio in a depth range of 600–1500 m is 3.1 ± 0.3, which is significantly lower than
495 that of 3.8 ± 0.2 below 3000 m. The low ratio in the intermediate depth could be attributed to the
496 dZn scavenging. In addition, the ratio in deep water exceeds the range of the Zn/PO_4 ratio in
497 phytoplankton, suggesting that additional dZn is supplied by the redissolution from sinking
498 particles and bottom sediments.

The dCu vs. PO_4 plot does not exhibit a linear relationship (Figure 5d). Instead, a general kink is observed at a depth of around 800 m, whereas the slopes are 0.20–0.41 mmol/mol for a depth range of 20–800 m (Table 1), which is close to the Cu/PO_4 ratio in phytoplankton (0.37–1.1 mmol/mol) (Bruland et al., 1991; Collier & Edmond, 1984; Ho et al., 2007; Kuss & Kremling, 1999). Instead, the dNi vs. PO_4 plot exhibits a linear relationship only in a depth range of 0–500 m (Figure 5b), and the slopes of 1.37–1.50 mmol/mol are close to the range of the Ni/PO_4 ratio in phytoplankton (0.22–1.4 mmol/mol) (Bruland et al., 1991; Collier & Edmond, 1984; Ho et al., 2007; Kuss & Kremling, 1999). The intercept is significantly higher at stations to the north of 40°N, suggesting a dNi supply from the northern continents (Figure 5b, Table 1). At a depth range of 500–2000 m, the data points are strongly curved, whereas dNi increases independently of PO_4 in a manner similar to dCu (gray shallow in Figure 5b). In deeper water, dNi decreases concurrently with PO_4 in a manner similar to dCd. However, the dZn vs. PO_4 plot exhibits a depletion of dZn from the surface to a 20 m depth and a linear relationship from 20 to 1000 m (Figure 5c). In a depth range of 1000–2000 m, dZn increases to its maximum independently of PO_4, like dNi (gray shallow in Figure 5c). Thus, it can be concluded that dNi and dZn at intermediate depth waters (200–2000 m) are not related to PO_4, whereas processes other than regeneration, such as the redissolution from sinking particles, probably play an important role on their distribution.

The abundance of lpCu is also a result of scavenging. The lpCu/tdCu ratio is 0.12 ± 0.05 (n = 227) in deep water (>1500 m) of the North Pacific Ocean, exhibiting a smaller deviation in deep waters than in the upper waters. Moreover, the lpCu/tdCu ratio is comparable to that for scavenged-type elements of Mn and Co, as discussed above. Cu is the only element among the four nutrient-type metals, whose lp species are broadly detected in the North Pacific Ocean. The large lpCu percentage can be explained by the adsorption of Cu onto particles, which is mainly controlled by the surface complexation (Li, 1981). The stability of the surface complexes exhibits a linear relationship with the first hydrolysis constant for the metal ion. Because the four metal ions in this study form divalent cations and Cu^{2+} has the highest first hydrolysis constant (Li, 1981), Cu exhibits the highest lpM/tdM ratio and the strongest scavenging. In contrast, Cd^{2+} has the lowest first hydrolysis constant, resulting in the weakest scavenging effect.

The scavenging of Ni has not been widely accepted yet. However, the residence time of dMs in the world ocean has been estimated to be 5,000 y for dCu (Boyle et al., 1977), 10,000–30,000 y for dNi (Cameron & Vance, 2014; Sclater, Boyle, & Edmond, 1976), 18,000 y for Zn (Bewers & Yeats, 1977), and 50,000 y for Cd (Boyle et al., 1976; Bruland, 1980). In addition, the scavenging residence time has been estimated to be 385 y for Cu, 15,850 y for Ni, and 177,800 y for Cd (Balistrieri, Brewer, & Murray, 1981). In the near-ridge environment, sedimentary Ni concentrations are increased due to the scavenging of Ni from seawater by Mn and Fe (oxyhydr)oxides (Costa et al., 2018; Dunk & Mills, 2006; Metz, Trefry, & Nelsen, 1988). Thus, we propose that scavenging is an important factor for Ni as well as for Cu and Zn.

4.3 Systematics in enrichment factor

The enrichment factor (EF) of dMs in seawater has been proposed in our previous reports (Zheng et al., 2019; Zheng & Sohrin, 2019) to clarify the sources/sinks of dMs:

$$EF(\mathrm{dM}) = (\mathrm{dM/dAl})_{\mathrm{seawater}}/(\mathrm{M/Al})_{\mathrm{upper\ crust}}$$

where $(M/Al)_{upper\ crust}$ represents the mole ratio in the upper crust (Rudnick & Gao, 2005). The box plots of *EF* for dFe, dissolved nutrient-type metals, and major nutrients in depths >300 m are presented in Figure 11. The median is 6.4 for dFe, 6.3×10^4 for dNi, 3.2×10^4 for dCu, 7.4×10^4 for dZn, 6.6×10^6 for dCd, 7.7×10^4 for $Si(OH)_4$, 7.1×10^5 PO_4, and 3.5×10^7 for NO_3. dCd exhibits the highest *EF* value among the four nutrient-type metals, which is one order of magnitude lower than that of NO_3, thus reflecting the lowest influence of scavenging on Cd. Furthermore, *EF*(dFe) is the lowest among the five metals, because dFe has been proven to be strongly affected by scavenging (Zheng & Sohrin, 2019). *EF*(dNi), *EF*(dCu), and *EF*(dZn) are in the same order of magnitude, which are two orders of magnitude lower than *EF*(dCd) but three orders of magnitude higher than *EF*(dFe). These results suggest that dNi, dCu, and dZn have a moderate interaction with particles.

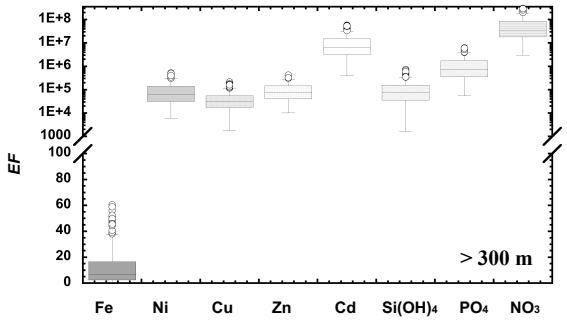

Figure 11. Box plots of *EF* for dFe, dNi, dCu, dZn, dCd, and major nutrients at depths > 300 m. The middle line of the box represents the median; the top and bottom lines of the box represent the upper and lower quartiles, respectively; and circles represent potential outliers.

It is possible that the solubility of Ms affects the *EF*(dMs). The solubility of the four metals and Al from aerosols deposited to the sea surface differs significantly depending on a series of factors, such as the aerosol sources (Chester et al., 1993) and the distance from the continent (Chester et al., 1993; Hsu et al., 2010; Mahowald et al., 2018). For example, the average solubility of the four metals and Al from the East China Sea aerosols are within a factor of 20 (Hsu et al., 2010). Thus, the solubility may not significantly affect the trend in Figure 11.

The horizontal distribution of *EF*(dCu) in the surface water implies that *EF*(dCu) is significantly high at stations within the North Pacific subarctic gyre (Figure S10a), whereas at stations ST14 and BD15, nearest to the Alaska Peninsula, *EF*(dCu) has a relatively low value compared with the surrounding stations. Moreover, the sectional distribution of *EF*(dCu) at 160°W reveals that the maximum occurs from the surface to a depth of 4000 m above 35°N (Figure S10b). *EF*(dNi), *EF*(dZn), and *EF*(dCd) also have similar distributions. dAl is as low as 0–0.5 nmol/kg in the surface water to the north of 40°N and is uniformly low through the water column above 26°N (Zheng et al., 2019), indicating the weak effect of the lithogenic sources in this area. The dCu vs. $Si(OH)_4$ plot with *EF*(dCu) in plot color shows that only data with *EF*(dCu) typically higher than 80,000 had a high correlation with $Si(OH)_4$ with a low slope of 0.00541 mmol/mol (Figure S10c). These samples are from waters shallower than 1500 m at stations to the north of 40°N. It has been reported that Cu from urban aerosols is more soluble than that from lithogenic aerosols (Chester et al., 1993). These results suggest that a large amount of anthropogenic Cu is supplied as aerosols to the northern North Pacific Ocean and is intensively scavenged from the water

column.

Consequently, we demonstrate that *EF*(dMs) can be a promising measure to decide whether or not an element is effectively scavenged through the water column, especially below the surface mixed layer. Since *EF*(dNi), *EF*(dCu), and *EF*(dZn) are comparable, we could infer that not only Cu but also Zn and Ni are affected by scavenging processes.

5 Conclusions

In this study, concurrent data of dissolved Cd, Ni, Zn, Cu, and labile particulate Cu that were collected during the GEOTRACES Japan cruises KH-05-2 (160°W), KH-11-7 (165°E), and KH-12-4 (47°N) in the north Pacific Ocean were reported. These data indicated that Cd is controlled by biogeochemical cycling and water mass circulation. Although Ni, Zn, and Cu are also controlled by biogeochemical cycling, they are affected by scavenging. Due to the internal formation of PDW in the North Pacific Ocean and its long residence time, the effects of scavenging for these metals can be detected. Each metal has a unique relationship with the major nutrients $Si(OH)_4$ and PO_4, whereas the dMs vs. nutrient plots strongly differ from those reported in other oceans. The dMs/PO_4 ratio, the *FF*(dCd), the preformed dCd (Cd^0), and the *EF*(dMs) can improve the understanding of the effect of biogeochemical cycles, scavenging, and redissolution on the distribution of the metals. Therefore, we revealed that among the four metals, Cu is the most affected by scavenging, whereas Cd is the least affected, and scavenging plays a significant role also on Ni and Zn.

Acknowledgments

The study was supported by KAKENHI grants (Grant Nos JP16204046, JP21350042, JP24241004, 15H01727, and 19H01148) from the Japan Society for the Promotion of Science, by Mitsumasa Ito Memorial Research Grants (H30-R3 and H31-R1) from the Research Institute for Oceanochemistry Foundation, by Sasakawa Scientific Research Grant (2019-3036) from the Japan Science Society, and by the International Collaborative Research Program (2019-47) from the Institute for Chemical Research, Kyoto University. We thank the crew, technicians, students, and scientists onboard the KH-05-2, KH-11-7, and KH-12-4 cruises for their assistance with sampling and analysis of routine parameters. We also thank ex-student Wataru Konagaya for his assistance in the determination of trace metals in some samples from KH-11-7 and KH-12-4. The raw data of this study are available in Table S3 for review process, and the data will be submitted to PANGAEA for archive.

References

Abe, K. (2001). Cd in the western equatorial Pacific. *Marine Chemistry, 74*(2-3), 197-211. doi:10.1016/s0304-4203(01)00015-9

Baars, O., Abouchami, W., Galer, S. J. G., Boye, M., & Croot, P. L. (2014). Dissolved cadmium in the Southern Ocean: Distribution, speciation, and relation to phosphate. *Limnology and Oceanography, 59*(2), 385-399.

Balistrieri, L., Brewer, P. G., & Murray, J. W. (1981). Scavenging residence times of trace metals and surface chemistry of sinking particles in the deep ocean. *Deep Sea Research Part A. Oceanographic Research Papers, 28*(2), 101-121. doi:10.1016/0198-0149(81)90085-6

Bewers, J. M., & Yeats, P. A. (1977). Oceanic residence times of trace metals. *Nature, 268*(5621), 595-598. doi:10.1038/268595a0

Bostock, H. C., Opdyke, B. N., & Williams, M. J. M. (2010). Characterising the intermediate depth waters of the Pacific Ocean using ∂ 13C and other geochemical tracers. *Deep Sea Research Part I: Oceanographic Research Papers, 57*(7), 847-859. doi:10.1016/j.dsr.2010.04.005

Boyle, E. A. (1988). Cadmium: Chemical Tracer of Deepwater Paleoceanography. *Paleoceanography, 3*(4), 471-489. doi:10.1029/PA003i004p00471

Boyle, E. A., Sclater, F., & Edmond, J. M. (1976). On the marine geochemistry of cadmium. *Nature, 263*(5572), 42-44.

Boyle, E. A., Sclater, F. R., & Edmond, J. M. (1977). The distribution of dissolved copper in the Pacific. *Earth and Planetary Science Letters, 37*(1), 38-54. doi:10.1016/0012-821X(77)90144-3

Broecker, W. S., & Peng, T.-H. (1982). *Tracers in the Sea* (Vol. 8). New York: Eldigio Press.

Bruland, K. W. (1980). Oceanographic distributions of cadmium, zinc, nickel, and copper in the North Pacific. *Earth and Planetary Science Letters, 47*(2), 176-198. doi:10.1016/0012-821x(80)90035-7

Bruland, K. W., Donat, J. R., & Hutchins, D. A. (1991). Interactive influences of bioactive trace metals on biological production in oceanic waters. *Limnology and Oceanography, 36*(8), 1555-1577. doi:10.4319/lo.1991.36.8.1555

Bruland, K. W., Orians, K. J., & Cowen, J. P. (1994). Reactive trace metals in the stratified central North Pacific. *Geochimica et Cosmochimica Acta, 58*(15), 3171-3182. doi:10.1016/0016-7037(94)90044-2

Cameron, V., & Vance, D. (2014). Heavy nickel isotope compositions in rivers and the oceans. *Geochimica et Cosmochimica Acta, 128*(0), 195-211. doi:10.1016/j.gca.2013.12.007

Chester, R., Murphy, K. J. T., Lin, F. J., Berry, A. S., Bradshaw, G. A., & Corcoran, P. A. (1993). Factors controlling the solubilities of trace metals from non-remote aerosols deposited to the sea surface by the 'dry' deposition mode. *Marine Chemistry, 42*(2), 107-126. doi:https://doi.org/10.1016/0304-4203(93)90241-F

Collier, R., & Edmond, J. (1984). The trace element geochemistry of marine biogenic particulate matter. *Progress in Oceanography, 13*(2), 113-199. doi:10.1016/0079-6611(84)90008-9

Conway, T. M., & John, S. G. (2015). Biogeochemical cycling of cadmium isotopes along a high-resolution section through the North Atlantic Ocean. *Geochimica et Cosmochimica Acta, 148*(0), 269-283. doi:10.1016/j.gca.2014.09.032

654 Costa, K. M., Anderson, R. F., McManus, J. F., Winckler, G., Middleton, J. L., & Langmuir, C.
655 H. (2018). Trace element (Mn, Zn, Ni, V) and authigenic uranium (aU) geochemistry
656 reveal sedimentary redox history on the Juan de Fuca Ridge, North Pacific Ocean.
657 *Geochimica et Cosmochimica Acta, 236*, 79-98.
658 doi:https://doi.org/10.1016/j.gca.2018.02.016
659 Croghan, C., & Egeghy, P. P. (2003). Methods of dealing with values below the limit of
660 detection using SAS. *Southern SAS User Group, 22*, 24.
661 Cullen, J. T. (2006). On the nonlinear relationship between dissolved cadmium and phosphate in
662 the modern global ocean: Could chronic iron limitation of phytoplankton growth cause
663 the kink? *Limnology and Oceanography, 51*(3), 1369-1380.
664 doi:10.4319/lo.2006.51.3.1369
665 Danielsson, L.-G., Magnusson, B., & Westerlund, S. (1985). Cadmium, copper, iron, nickel and
666 zinc in the north-east Atlantic Ocean. *Marine Chemistry, 17*(1), 23-41.
667 doi:https://doi.org/10.1016/0304-4203(85)90034-9
668 de Baar, H. J. W., Saager, P. M., Nolting, R. F., & van der Meer, J. (1994). Cadmium versus
669 phosphate in the world ocean. *Marine Chemistry, 46*(3), 261-281. doi:10.1016/0304-
670 4203(94)90082-5
671 Dunk, R. M., & Mills, R. A. (2006). The impact of oxic alteration on plume-derived transition
672 metals in ridge flank sediments from the East Pacific Rise. *Marine Geology, 229*(3), 133-
673 157. doi:https://doi.org/10.1016/j.margeo.2006.03.007
674 Elderfield, H. (Ed.) (2003). *The Oceans and Marine Geochemistry*. Oxford: Elsevier-Pergamon.
675 Elderfield, H., & Rickaby, R. E. M. (2000). Oceanic Cd/P ratio and nutrient utilization in the
676 glacial Southern Ocean. *Nature, 405*(6784), 305-310.
677 Ellwood, M. J., & Hunter, K. A. (2000). The incorporation of zinc and iron into the frustule of
678 the marine diatom Thalassiosira pseudonana. *Limnology and Oceanography, 45*(7), 1517-
679 1524. doi:10.4319/lo.2000.45.7.1517
680 Emerson, S. R., & Hedges, J. I. (2008). *Chemical Oceanography and the Marine Carbon Cycle*.
681 Cambridge: Cambridge University Press.
682 Fischer, K., Dymond, J., Lyle, M., Soutar, A., & Rau, S. (1986). The benthic cycle of copper:
683 Evidence from sediment trap experiments in the eastern tropical North Pacific Ocean.
684 *Geochimica et Cosmochimica Acta, 50*(7), 1535-1543. doi:10.1016/0016-7037(86)90327-
685 3
686 Frew, R. D., & Hunter, K. A. (1992). Influence of Southern Ocean waters on the cadmium-
687 phosphate properties of the global ocean. *Nature, 360*(6400), 144-146.
688 Frew, R. D., & Hunter, K. A. (1995). Cadmium-phosphorus cycling at the subtropical
689 convergence south of New Zealand. *Marine Chemistry, 51*(3), 223-237.
690 doi:https://doi.org/10.1016/0304-4203(95)00057-7
691 Goldberg, E. D. (1954). Marine Geochemistry 1. Chemical Scavengers of the Sea. *The Journal
692 of Geology, 62*(3), 249-265. doi:10.2307/30080120
693 Heller, M. I., & Croot, P. L. (2015). Copper speciation and distribution in the Atlantic sector of
694 the Southern Ocean. *Marine Chemistry, 173*, 253-268.
695 doi:https://doi.org/10.1016/j.marchem.2014.09.017
696 Ho, T.-Y., Wen, L. S., You, C. F., & Lee, D. C. (2007). The trace-metal composition of size-
697 fractionated plankton in the South China Sea: Biotic versus abiotic sources. *Limnology
698 and Oceanography, 52*(5), 1776-1788.

699 Ho, T.-Y., You, C.-F., Chou, W.-C., Pai, S.-C., Wen, L.-S., & Sheu, D. D. (2009). Cadmium and
700 phosphorus cycling in the water column of the South China Sea: The roles of biotic and
701 abiotic particles. *Marine Chemistry, 115*(1-2), 125-133.
702 Hsu, S.-C., Wong, G. T. F., Gong, G.-C., Shiah, F.-K., Huang, Y.-T., Kao, S.-J., . . . Tseng, C.-
703 M. (2010). Sources, solubility, and dry deposition of aerosol trace elements over the East
704 China Sea. *Marine Chemistry, 120*(1-4), 116-127.
705 Jacquot, J. E., & Moffett, J. W. (2015). Copper distribution and speciation across the
706 International GEOTRACES Section GA03. *Deep Sea Research Part II: Topical Studies*
707 *in Oceanography, 116*(0), 187-207. doi:10.1016/j.dsr2.2014.11.013
708 Janssen, D. J., Abouchami, W., Galer, S. J. G., Purdon, K. B., & Cullen, J. T. (2019). Particulate
709 cadmium stable isotopes in the subarctic northeast Pacific reveal dynamic Cd cycling and
710 a new isotopically light Cd sink. *Earth and Planetary Science Letters, 515*, 67-78.
711 doi:https://doi.org/10.1016/j.epsl.2019.03.006
712 Janssen, D. J., Conway, T. M., John, S. G., Christian, J. R., Kramer, D. I., Pedersen, T. F., &
713 Cullen, J. T. (2014). Undocumented water column sink for cadmium in open ocean
714 oxygen-deficient zones. *Proceedings of the National Academy of Sciences, 111*(19),
715 6888-6893. doi:10.1073/pnas.1402388111
716 Janssen, D. J., & Cullen, J. T. (2015). Decoupling of zinc and silicic acid in the subarctic
717 northeast Pacific interior. *Marine Chemistry, 177, Part 1*, 124-133.
718 doi:10.1016/j.marchem.2015.03.014
719 John, S. G., & Conway, T. M. (2014). A role for scavenging in the marine biogeochemical
720 cycling of zinc and zinc isotopes. *Earth and Planetary Science Letters, 394*, 159-167.
721 doi:https://doi.org/10.1016/j.epsl.2014.02.053
722 Kim, T., Obata, H., Kondo, Y., Ogawa, H., & Gamo, T. (2015). Distribution and speciation of
723 dissolved zinc in the western North Pacific and its adjacent seas. *Marine Chemistry, 173*,
724 330-341. doi:10.1016/j.marchem.2014.10.016
725 Kim, T., Obata, H., Nishioka, J., & Gamo, T. (2017). Distribution of Dissolved Zinc in the
726 Western and Central Subarctic North Pacific. *Global Biogeochemical Cycles, 31*(9),
727 1454–1468. doi:10.1002/2017GB005711
728 Kudo, I., Kokubun, H., & Matsunaga, K. (1996). Cadmium in the southwest Pacific Ocean two
729 factors significantly affecting the Cd–PO4 relationship in the ocean. *Marine Chemistry,*
730 *54*(1), 55-67. doi:https://doi.org/10.1016/0304-4203(95)00100-X
731 Kuss, J., & Kremling, K. (1999). Spatial variability of particle associated trace elements in near-
732 surface waters of the North Atlantic (30°N/60°W to 60°N/2°W), derived by large volume
733 sampling. *Marine Chemistry, 68*(1-2), 71-86. doi:10.1016/s0304-4203(99)00066-3
734 Laanemets, J., Kononen, K., Pavelson, J., & Poutanen, E. L. (2004). Vertical location of seasonal
735 nutriclines in the western Gulf of Finland. *Journal of Marine Systems, 52*(1), 1-13.
736 doi:https://doi.org/10.1016/j.jmarsys.2004.03.003
737 Li, Y.-H. (1981). Ultimate removal mechanisms of elements from the ocean. *Geochimica et*
738 *Cosmochimica Acta, 45*(10), 1659-1664. doi:10.1016/0016-7037(81)90001-6
739 Little, S. H., Vance, D., Siddall, M., & Gasson, E. (2013). A modeling assessment of the role of
740 reversible scavenging in controlling oceanic dissolved Cu and Zn distributions. *Global*
741 *Biogeochemical Cycles*, n/a-n/a. doi:10.1002/gbc.20073
742 Löscher, B. M., de Jong, J. T. M., & de Baar, H. J. W. (1998). The distribution and preferential
743 biological uptake of cadmium at 6°W in the Southern Ocean. *Marine Chemistry, 62*(3–4),
744 259-286. doi:10.1016/S0304-4203(98)00045-0

Löscher, B. M., van der Meer, J., de Baar, H. J. W., Saager, P. M., & de Jong, J. T. M. (1997). The global Cd/phosphate relationship in deep ocean waters and the need for accuracy. *Marine Chemistry, 59*(1), 87-93. doi:https://doi.org/10.1016/S0304-4203(97)00067-4

Mahowald, N. M., Hamilton, D. S., Mackey, K. R. M., Moore, J. K., Baker, A. R., Scanza, R. A., & Zhang, Y. (2018). Aerosol trace metal leaching and impacts on marine microorganisms. *Nature Communications, 9*(1), 2614. doi:10.1038/s41467-018-04970-7

Metz, S., Trefry, J. H., & Nelsen, T. A. (1988). History and geochemistry of a metalliferous sediment core from the Mid-Atlantic Ridge at 26°N. *Geochimica et Cosmochimica Acta, 52*(10), 2369-2378. doi:https://doi.org/10.1016/0016-7037(88)90294-3

Middag, R., van Heuven, S. M. A. C., Bruland, K. W., & de Baar, H. J. W. (2018). The relationship between cadmium and phosphate in the Atlantic Ocean unravelled. *Earth and Planetary Science Letters, 492*, 79-88. doi:https://doi.org/10.1016/j.epsl.2018.03.046

Minami, T., Konagaya, W., Zheng, L., Takano, S., Sasaki, M., Murata, R., . . . Sohrin, Y. (2015). An off-line automated preconcentration system with ethylenediaminetriacetate chelating resin for the determination of trace metals in seawater by high-resolution inductively coupled plasma mass spectrometry. *Analytica Chimica Acta, 854*(0), 183-190. doi:10.1016/j.aca.2014.11.016

Monteiro, P. M. S., & Orren, M. J. (1985). Trace metals in the Southern Ocean: on the geochemistry of copper. *Marine Chemistry, 15*(4), 345-355. doi:10.1016/0304-4203(85)90045-3

Noriki, S., & Tsunogai, S. (1992). Directly observed particulate fluxes of Cd, Ni and Cu in pelagic oceans: implication of two different settling particles. *Marine Chemistry, 37*(1), 105-115. doi:https://doi.org/10.1016/0304-4203(92)90059-J

Quay, P., Cullen, J., Landing, W., & Morton, P. (2015). Processes controlling the distributions of Cd and PO4 in the ocean. *Global Biogeochemical Cycles, 29*(6), 830-841.

Redfield, A. C., Ketchum, B. H., & Richards, F. A. (1963). The influence of organisms on the composition of sea-water. In M. N. Hill (Ed.), *The Sea* (Vol. 2, pp. 26-77). New York: Wiley.

Roshan, S., & Wu, J. (2015a). Cadmium regeneration within the North Atlantic. *Global Biogeochemical Cycles, 29*(12), 2082-2094.

Roshan, S., & Wu, J. (2015b). The distribution of dissolved copper in the tropical-subtropical north Atlantic across the GEOTRACES GA03 transect. *Marine Chemistry, 176*, 189-198. doi:10.1016/j.marchem.2015.09.006

Roshan, S., & Wu, J. (2018). Dissolved and colloidal copper in the tropical South Pacific. *Geochimica et Cosmochimica Acta, 233*, 81-94. doi:https://doi.org/10.1016/j.gca.2018.05.008

Rudnick, R. L., & Gao, S. (2005). Composition of the continental crust. In R. L. Rudnick (Ed.), *The Crust* (pp. 1-64). Oxford: Elsevier-Pergamon.

Saager, P. M., De Baar, H. J. W., & Howland, R. J. (1992). Cd, Zn, Ni and Cu in the Indian Ocean. *Deep Sea Research Part A. Oceanographic Research Papers, 39*(1), 9-35. doi:10.1016/0198-0149(92)90017-n

Sarmiento, J. L., & Gruber, N. (2006). *Ocean Biogeochemical Dynamics*. Princeton: Princeton University Press.

Schlitzer, R. (2015). Ocean Data View. *odv.awi.de*.

Schlitzer, R., Anderson, R. F., Dodas, E. M., Lohan, M., Geibert, W., Tagliabue, A., . . . Zurbrick, C. (2018). The GEOTRACES Intermediate Data Product 2017. *Chemical Geology, 493*, 210-223. doi:https://doi.org/10.1016/j.chemgeo.2018.05.040

Sclater, F. R., Boyle, E., & Edmond, J. M. (1976). On the marine geochemistry of nickel. *Earth and Planetary Science Letters, 31*(1), 119-128. doi:10.1016/0012-821X(76)90103-5

Sherrell, R. M., & Boyle, E. A. (1992). The trace metal composition of suspended particles in the oceanic water column near Bermuda. *Earth and Planetary Science Letters, 111*, 155-174.

Sunda, W. (2012). Feedback Interactions between Trace Metal Nutrients and Phytoplankton in the Ocean. *Frontiers in Microbiology, 3*, 204.

Sunda, W. G. (1989). Trace Metal Interactions with Marine Phytoplankton. *Biological Oceanography, 6*(5-6), 411-442. doi:10.1080/01965581.1988.10749543

Takano, S., Tanimizu, M., Hirata, T., & Sohrin, Y. (2014). Isotopic constraints on biogeochemical cycling of copper in the ocean. *Nat Commun, 5*. doi:10.1038/ncomms6663

Talley, L. D. (1993). Distribution and Formation of North Pacific Intermediate Water. *Journal of Physical Oceanography, 23*(3), 517-537. doi:10.1175/1520-0485(1993)023<0517:DAFONP>2.0.CO;2

Talley, L. D., Pickard, G. L., Emery, W. J., & Swift, J. H. (2011). *Descriptive Physical Oceanography: An Introduction* (6th ed.). Amsterdam: Elsevier.

Twining, B. S., & Baines, S. B. (2013). The Trace Metal Composition of Marine Phytoplankton. *Annual Review of Marine Science, 5*(1), 191-215. doi:10.1146/annurev-marine-121211-172322

van der Loeff, M. R., Helmers, E., & Kattner, G. (1997). Continuous transects of cadmium, copper, and aluminium in surface waters of the Atlantic Ocean, 50°N to 50°S: Correspondance and contrast with nutrient-like behaviour. *Geochimica et Cosmochimica Acta, 61*, 47-61.

Vance, D., de Souza, G. F., Zhao, Y., Cullen, J. T., & Lohan, M. C. (2019). The relationship between zinc, its isotopes, and the major nutrients in the North-East Pacific. *Earth and Planetary Science Letters, 525*, 115748. doi:https://doi.org/10.1016/j.epsl.2019.115748

Vance, D., Little, S. H., de Souza, G. F., Khatiwala, S., Lohan, M. C., & Middag, R. (2017). Silicon and zinc biogeochemical cycles coupled through the Southern Ocean. *Nature Geosci, advance online publication*. doi:10.1038/ngeo2890

http://www.nature.com/ngeo/journal/vaop/ncurrent/abs/ngeo2890.html#supplementary-information

Vu, H. T. D., & Sohrin, Y. (2013). Diverse stoichiometry of dissolved trace metals in the Indian Ocean. *Scientific Reports, 3*, 1745. doi:10.1038/srep01745

Wang, R. M., Archer, C., Bowie, A. R., & Vance, D. (2019). Zinc and nickel isotopes in seawater from the Indian Sector of the Southern Ocean: The impact of natural iron fertilization versus Southern Ocean hydrography and biogeochemistry. *Chemical Geology, 511*, 452-464. doi:https://doi.org/10.1016/j.chemgeo.2018.09.010

Weber, T., John, S., Tagliabue, A., & DeVries, T. (2018). Biological uptake and reversible scavenging of zinc in the global ocean. *Science, 361*(6397), 72-76.

Whitfield, M., & Turner, D. R. (1987). The Role of Particles in Regulating the Composition of Seawater. In W. Stumm (Ed.), *Aquatic Surface Chemistry* (pp. 457-493). New York: John Wiley & Sons.

Wu, J., & Roshan, S. (2015). Cadmium in the North Atlantic: Implication for global cadmium–phosphorus relationship. *Deep Sea Research Part II: Topical Studies in Oceanography, 116*(0), 226-239. doi:10.1016/j.dsr2.2014.11.007

Xie, R. C., Galer, S. J. G., Abouchami, W., Rijkenberg, M. J. A., De Jong, J., de Baar, H. J. W., & Andreae, M. O. (2015). The cadmium–phosphate relationship in the western South Atlantic — The importance of mode and intermediate waters on the global systematics. *Marine Chemistry, 177, Part 1*, 110-123. doi:http://dx.doi.org/10.1016/j.marchem.2015.06.011

Yang, S.-C., Zhang, J., Sohrin, Y., & Ho, T.-Y. (2018). Cadmium cycling in the water column of the Kuroshio-Oyashio Extension region: Insights from dissolved and particulate isotopic composition. *Geochimica et Cosmochimica Acta, 233*, 66-80. doi:https://doi.org/10.1016/j.gca.2018.05.001

Yasuda, I. (1997). The origin of the North Pacific intermediate water. *Journal of Geophysical Research: Oceans, 102*(C1), 893-909.

Yasuda, I. (2003). Hydrographic Structure and Variability in the Kuroshio-Oyashio Transition Area. *Journal of Oceanography, 59*(4), 389-402. doi:10.1023/A:1025580313836

Yuan, X., & Talley, L. D. (1996). The subarctic frontal zone in the North Pacific: Characteristics of frontal structure from climatological data and synoptic surveys. *Journal of Geophysical Research: Oceans, 101*(C7), 16491-16508. doi:10.1029/96JC01249

Zhang, R., Jensen, L. T., Fitzsimmons, J. N., Sherrell, R. M., & John, S. (2019). Dissolved cadmium and cadmium stable isotopes in the western Arctic Ocean. *Geochimica et Cosmochimica Acta, 258*, 258-273. doi:https://doi.org/10.1016/j.gca.2019.05.028

Zheng, L., Minami, T., Konagaya, W., Chan, C.-Y., Tsujisaka, M., Takano, S., . . . Sohrin, Y. (2019). Distinct basin-scale-distributions of aluminum, manganese, cobalt, and lead in the North Pacific Ocean. *Geochimica et Cosmochimica Acta, 254*, 102-121. doi:https://doi.org/10.1016/j.gca.2019.03.038

Zheng, L., & Sohrin, Y. (2019). Major lithogenic contributions to the distribution and budget of iron in the North Pacific Ocean. *Scientific Reports, 9*(1), 11652. doi:10.1038/s41598-019-48035-1